Proceedings of the Thirty-second (2022) International Ocean and Polar Engineering Conference **www.isope.org**
Shanghai, China, June 5–10, 2022

ISBN 978-1-880653-81-4; ISSN 1098-6189

Numerical study of flow around a three-dimensional elastic cylinder based on coupled CFD-FEM method

Wenjie Zhang[1], Jianhua Wang[1], Yi Liu[2], Hao Guo[2], Decheng Wan[1]*
1. Computational Marine Hydrodynamics Lab (CMHL), School of Naval Architecture, Ocean and Civil Engineering, Shanghai Jiao Tong University, Shanghai, China
2. Marine Design and Research Institute of China, Shanghai, China
* Corresponding Author

ABSTRACT

In practical engineering, the long and thin blunt structures are able to produce non-negligible deformation and periodic vibration under the strong influence of intense incoming flow. In the present work, a strong coupling approach is developed based on CFD-FEM method to solve the FSI problem. Fluid field is solved by RANS method with OpenFOAM. Structural vibration is solved by Newmark-beta method, which is based on Euler-Bernoulli beam model. Computational mesh updating strategy is adopted to realize the dynamic mesh updating to consider the effect of structural vibration deformation. In this paper, a numerical study of flow around a three-dimensional elastic cylinder under stokes second order wave is investigated to validate the developed FSI solver. In order to study the wave frequencies effect on the phenomenon of flow around elastic cylinders, three different wave frequencies are investigated for a three-dimensional elastic cylinder. Structural response and fluid analysis, i.e., wave profiles and vorticity field are presented. The accuracy and stability of developed CFD-FEM approach are demonstrated through the numerical studies preliminarily.

KEY WORDS: Fluid-structure interaction (FSI), Three-dimensional elastic cylinder, Vibration deformation, CFD-FEM approach.

INTRODUCTION

The model studied in this paper has a wide range of applications in the study of sediment dynamics in open channel flow. The model is commonly used in the research background of riparian water-level-fluctuation zone, erosion ditch, slope water movement around vegetation and so on (Zhang, 1989, Ebrahim, 2018). The structures are generally regarded as rigid and rigid with no deformation to simplify the research problems. Many scholars has focused on the horseshoe vortex structure before the cylinder in open channel flow, and regard the structure blocking the flow as rigid (Dargahi, 1989, Qi, 2005, Euler, 2012, Tafarojnoruz, 2010). Chen and Yang have carried out flow experiments on the flow around a cylinder under shallow water in an open channel flume, and studied the kinematic characteristics of horseshoe vortices upstream of open channel cylinders (Chen, 2016, Yang, 2019). Nikolaos has studied the physical characteristics of turbulent separation near the vertical intersection of a flat wall and a cylindrical obstacle with both experimental and numerical methods (Nikolaos, 2015). This simplification is feasible for bridge pier structure, but not accurate for slope water movement around vegetation and some other problems.

The introduction of CFD-FEM provides an effective method to study cylinder deformation. Bending deformation of a cylinder in single phase flow has a wide engineering background, among which the typical application is wind resistance of high-rise buildings. Many scholars have carried out research on both model experiments and numerical simulations (Waldeck, 1992, Larsen, 1995, Ciesielski, 1996, Facchinetti, 2004, Zhang, 2005, Liang, 2019, Francesca, 2021). Similar research work in two phase flow is relatively rare.

This paper takes an elastic cantilever cylinder model as the research object. Firstly, the stability of developed FSI solver is preliminarily verified by grid convergence analysis. The FSI numerical simulations between waves at different frequencies and fixed elastic cantilever cylinder are carried out. Both structure vibration displacement response of elastic cylinder and fluid field characteristics of wave profiles and vorticity field are studied. The research is expected to contribute to the understanding of FSI problems.

THE MATHEMATICAL FORMULATIONS

Governing Equations

The flow is assumed as incompressible, and energy transformation caused by temperature change is ignored. For applications of engineering problems, the governing equation of the flow field adopts Reynolds average equation:

$$\frac{\partial \overline{u_i}}{\partial x_i} = 0 \tag{1}$$

$$\frac{\partial \bar{u}_i}{\partial t}+\frac{\partial \bar{u}_i \bar{u}_j}{\partial x_j}=-\frac{1}{\rho}\frac{\partial \bar{p}}{\partial x_i}+\frac{\partial}{\partial x_j}\left[v\left(\frac{\partial \bar{u}_i}{\partial x_j}+\frac{\partial \bar{u}_j}{\partial x_i}\right)\right]-\frac{1}{\rho}\frac{\partial \tau_{ij}}{\partial x_j} \tag{2}$$

Reynolds stress term, $\tau_{ij}=\rho\overline{u_i' u_j'}$, is generated by pulsation velocity and represents turbulence effect. The relationship between Reynolds stress and average velocity gradient can be established after the introduction of the viscous vortex hypothesis:

$$\tau_{ij}=\rho\overline{u_i' u_j'}=-\mu_t\left(\frac{\partial \bar{u}_i}{\partial x_j}+\frac{\partial \bar{u}_j}{\partial x_i}\right)+\frac{2}{3}\left(\rho k+\mu_t\frac{\partial \bar{u}_i}{\partial x_i}\right)\delta_{ij} \tag{3}$$

where k is turbulent kinetic energy term. It is necessary to introduce a suitable turbulence model to determine the turbulence viscosity coefficient μ_t, so that the equations can be closed. The shear stress transport *SST* $k-\omega$ model is used in this study. The $k-\omega$ turbulence model is used to deal with the flow within the boundary layer on the near wall surface, and the $k-\varepsilon$ turbulence model is used to deal with the flow at the boundary layer edge and outside of the boundary layer. This model has the advantages of wide application range, high precision and wide application.

Stokes Second Order Wave

In this paper, stokes second order wave is taken for numerical wave generation (Dean, 1991). The potential function and wave surface function of stokes second order wave are:

$$\phi=\frac{\pi H}{kT}\frac{\cosh[k(z+h)]}{\sinh(kh)}\sin(kx-\sigma t)+\frac{3}{8}\frac{\pi^2 H}{kT}\left(\frac{H}{L}\right)\frac{\cosh[2k(z+h)]}{\sinh^4(kh)}\sin 2(kx-\sigma t) \tag{4}$$

$$\eta=\frac{H}{2}\cos(kx-\sigma t)+\frac{\pi H}{8}\left(\frac{H}{L}\right)\frac{\cosh(kh)\cdot[\cos(2kh)+2]}{\sinh^3(kh)}\cos 2(kx-\sigma t) \tag{5}$$

Newmark-beta Method

The structure uses an Euler-Bernoulli cantilever model fixed at one end. The structural dynamics equation is:

$$[M][\ddot{x}]+[C][\dot{x}]+[K][x]=[F] \tag{6}$$

where $[M]$, $[C]$, $[K]$ and $[F]$ are mass matrix, damping matrix, stiffness matrix and load vector respectively. In this paper, damping matrix adopts the form of Rayleigh damping. $[x]$, $[\dot{x}]$ and $[\ddot{x}]$ are generalized displacement, velocity and acceleration vectors containing linear and angular deformation respectively.

The Newmark-beta method was used to solve the structural dynamic equations. The deformation of the position of node (i+1) can be explicitly calculated by the displacement, velocity, acceleration vector of the node i and other known quantities:

$$\hat{K}x_{i+1}=\hat{F}_{i+1} \tag{7}$$

where:

$$\hat{K}=K+\frac{1}{\beta(\Delta t)^2}M+\left(\frac{\delta}{\beta(\Delta t)}\right)C \tag{8}$$

$$\hat{F}_{i+1}=F_{i+1}+\left[\frac{1}{\beta(\Delta t)^2}x_i+\frac{1}{\beta(\Delta t)}\dot{x}_i+\left(\frac{1}{2\beta}-1\right)\ddot{x}_i\right]M+\left[\frac{\delta}{\beta(\Delta t)}x_i+\left(\frac{\delta}{\beta}-1\right)\dot{x}_i+\frac{\Delta t}{2}\left(\frac{\delta}{\beta}-2\right)\ddot{x}_i\right]C \tag{9}$$

The constant parameters β and δ are determined by experience.

Fluid Structure Interaction Method

The fluid structure interaction method adopted in this paper is bidirectional fluid-structure coupling. Firstly, topoSet tool in OpenFOAM was used to extract the cantilever beam surface mesh of different segments, and the force integration of the mesh elements was carried out to obtain the concentrated force acting on the segment. Then, cubic spline interpolation is performed to calculate the distributed forces acting on each beam segment and to calculate the structural deformation. After that, the cubic spline function interpolation was also used to obtain the coordinate displacement information of the structure surface grid nodes, and the node coordinates of the fitting grid were updated. Finally, the flow field was used to calculate the mesh update. The flow chart of the above process is as shown in Fig. 1.

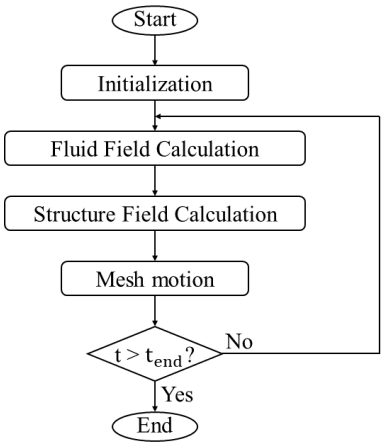

Fig. 1 Fluid structure coupling process

NUMERICAL SETUP

Geometric Model

In this paper, an elastic vertical cantilever cylinder is selected as the geometric model, as shown in Fig. 2. The diameter d=1 m, the cylinder length L=10 m, the mean surface height h=5 m, the amplitude of wave is 0.3 m, the bending stiffness of cylinder is EI= $1\times10^7 N\cdot m^2$ .The calculation parameter settings are shown in Table 1.

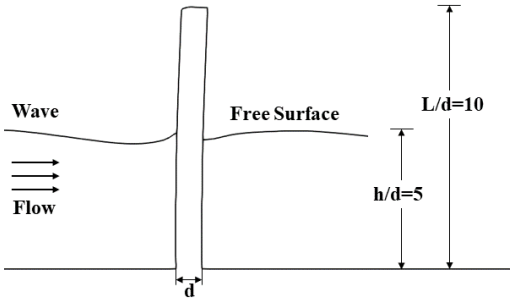

Fig. 2 Geometric model of the studying problem

Table 1. The basic parameters of the cavitation calculation

Cylinder parameters	Value
Diameter	1 m
Length	10 m
Bending stiffness	$1 \times 10^7 N \cdot m^2$
Mean surface height	5 m
Wave amplitude	0.3 m

Computing Domain Setup

The inlet is 10D from cylinder, the outlet is 20D from cylinder, and each side is 10D away from cylinder, as shown in Fig. 3. The atmosphere is about 15D away from free surface. Second-order stokes waves with different wave lengths are introduced into the computational domain from inlet with velocity of 2m/s. The velocity of uniform flow is 2m/s and the Reynolds Number is Re= 4×10^6. The velocity boundary condition of inlet patch is waveVelocity and that of outlet is outletPhaseMeanVelocity. Pressure boundary condition of inlet is fixedFluxPressure and that of outlet patch is zeroGradient.

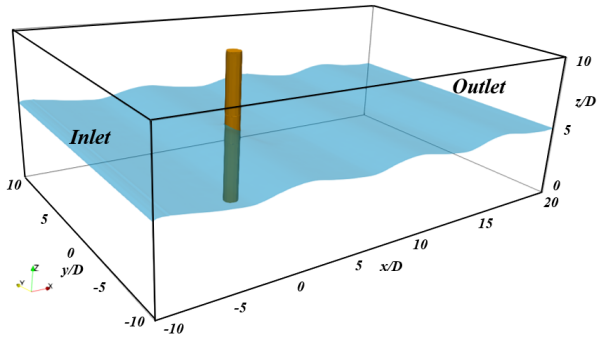

Fig. 3 Computational domain

The computational domain is discretized into unstructured grid. Besides, 3 levels of refinement are set up for meshes near the cylinder. Additional refinement is set in the free surface area to capture wave surface accurately, as shown in Fig. 4.

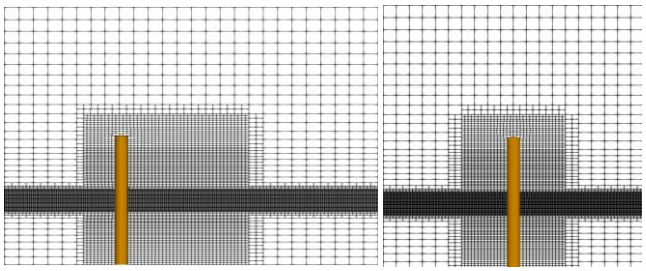

Fig. 4 Grid section of computational dimain

RESULTS AND DISCUSSIONS

Grid convergence verification

In order to perform preliminary verification of the developed FSI solver, grid convergence analysis is carried out for an example with a wave length of 8m incident wave. The grid quantity of coarse case is 0.7 million, that of medium case is 1.0 million, and that of fine case is 1.4 million. The time history curves of cylinder top displacement along inline direction are shown in Fig. 5.

At the initial moment, both wave and current make a relative large displacement along inline direction, resulting in a large elastic recovery force of the cylinder. Then the elastic recovery force overcomes fluid forces and produces recovery motion, forming a large oscillation motion at the end of the cylinder. However, the amplitude of vibration gradually decreases and stabilizes by the influence of damping.

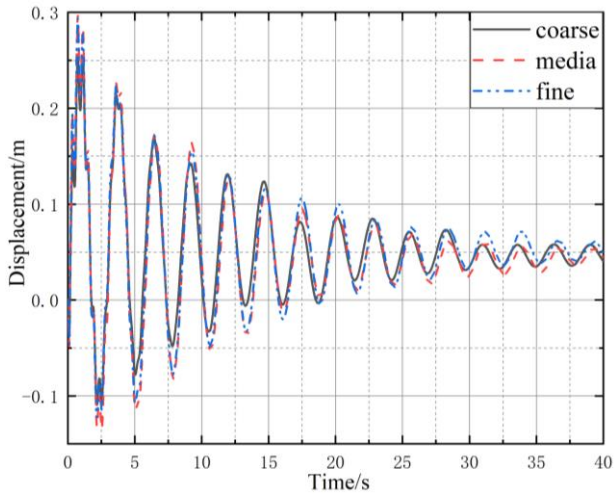

Fig. 5 Time history of cylinder top displacement along inline direction

It can be seen from Fig. 5 that the calculation grids of different scales have little influence on the calculation of structural displacement. The convergence results of structural displacement calculation are good in different computational meshes. Thus, the convergence calculation initially verifies the reliability of the FSI solver. Considering the balance between calculation accuracy and efficiency, the computational grid with medium quantity is used to carry out calculation cases below.

Structural Analysis

In this paper, the interaction between waves with different frequencies and elastic cylinder is studied under same wave amplitude by changing

the wave length. Time history of cylinder top vibration displacement along inline and crossflow directions of three different frequencies waves cases is shown in Fig. 6. Wave period of corresponding wave length are shown in Table 2.

Table 2. Wave period of corresponding wave length

Wave length	Wave period
8 m	2.26 s
12 m	2.79 s
16 m	3.26 s

It is clear that the oscillations in the inline direction are more periodic than those in the crossflow direction. When both wave and current exist at the same time and the wave amplitude is small, different wave frequencies have little effect on the inline amplitude after the column vibration is stabilized. When the wavelength is 12m, the wave frequency is close to the first-order natural frequency of the cylinder, but the result of the example with wavelength of 8m in the displacement time-history curve is similar to that of the example with wavelength of 12m. This may be due to the interaction between the flow field and the structure changing the natural frequency of the cylinder vibrating in the fluid. When the wave wavelength is 16m, it can be seen that the periodic vibration amplitude of the structure decreases obviously. The vibration displacement along crossflow direction vibrates around zero with the amplitude much smaller than that along inline direction.

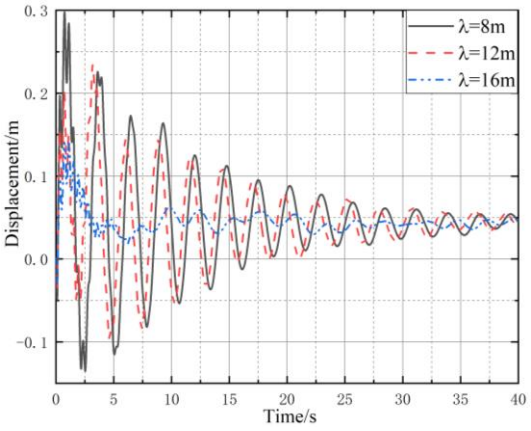

(a) Inline

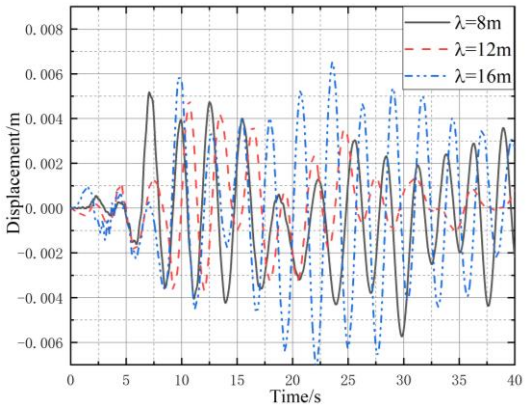

(b) Crossflow

Fig. 6 Time history of cylinder top vibration displacement

Fast Fourier analysis was performed on the above time history results, as shown in Fig. 7. It can be seen that different wave frequencies do not have much influence on the main vibration frequency of the cylinder. The vibration frequency of elastic cylinder is quite consistent for inline direction vibrations. For vibrations along crossflow direction, the vibration frequency of elastic cylinder is slightly different, but the difference is very small. The main frequency of inline vibration is quite close to that of crossflow vibration.

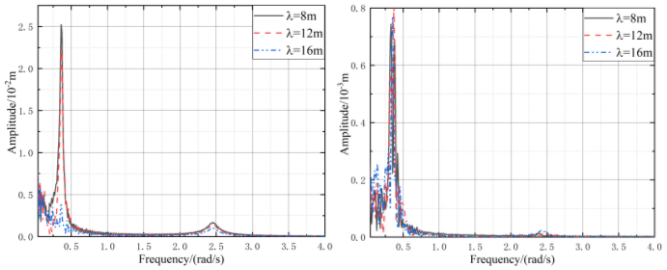

Fig. 7 FFT results of cylinder top vibration displacement time history

Hydrodynamic Analysis

Since waves of different wave lengths have little influence on the analysis of hydrodynamic characteristics of the fluid field, the calculation results of waves with a wavelength of 0.8m will be taken as an example for subsequent analysis. The isoline of instantaneous wave surface is extracted and fluid field is colored by wave height, as shown in Fig. 8. It is evident that the wave height has a run-up ahead of the cylinder and has a depression behind it.

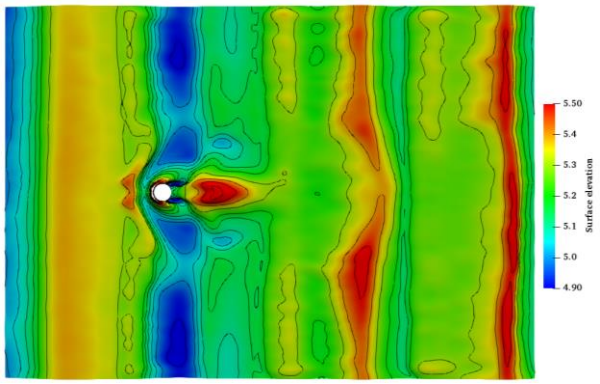

Fig. 8 Instantaneous surface elevation

Due to the existence of uniform flow and elastic cylinder structure, the development of wave surface is affected. It's clear that the trough decrease of wave is more obvious near the cylinder than that in other positions of the fluid field. The distribution of flow field in the computational domain is still symmetric as the low velocity of uniform flow and wave.

The velocity vector for the underwater flow field is extracted, as shown in Fig. 9. It is clear that there is an obvious backflow behind the cylinder and the velocity is mainly distributed horizontally in the flow field under the wave surface by the influence of uniform flow. Therefore, with the development of waves, the wave surface fluctuation will be gradually affected and decreased by the uniform flow at the bottom, so that the amplitude of wave surface fluctuation will be further reduced, and the

flow field ultimately developed is dominated by uniform flow. This is also why in Fig. 6 the vibration time history of the structure along inline direction doesn't show the vibration characteristic related to the wave period.

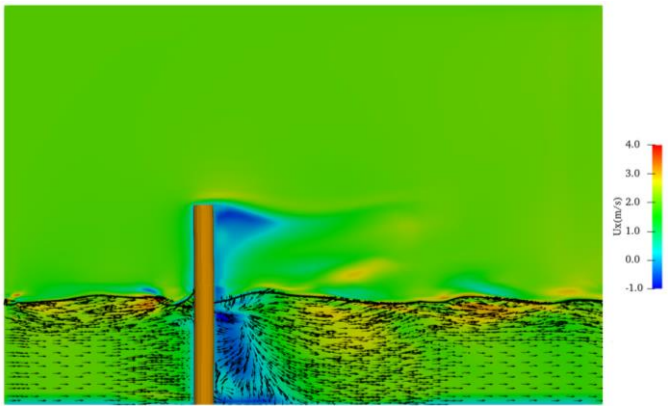

Fig. 9 Velocity field distribution underwater

Fig. 10 shows the vorticity distribution of flow field at different heights colored by Liutex, a modified normalized vortex identification method (Liu, 2019). The definition of vortex OmegaR is:

$$\Omega_R = \frac{(\vec{w}\cdot\vec{r})^2}{2\left[(\vec{w}\cdot\vec{r})^2 - 2\lambda_{ci}^2 + 2\lambda_{cr}^2 + \lambda_r^2\right] + \epsilon} \tag{10}$$

where $\vec{w}$ represents the vorticity and $\vec{r}$ represents the direction of local rotational axis of vortex. $\lambda_{cr} \pm \lambda_{ci} i$ are complex conjugate eigenvalues of velocity gradient tensor $\nabla\vec{v}$, λ_r is real eigenvalue of $\nabla\vec{v}$ and ϵ is a small parameter to prevent computational noise.

It's clear that the vorticity at some certain depth underwater is larger than that at the water surface, indicating that the waves on the water surface and the uniform flow underwater will produce intense mixing, resulting in obvious vortex structures. This feature can also be verified in Fig. 11.

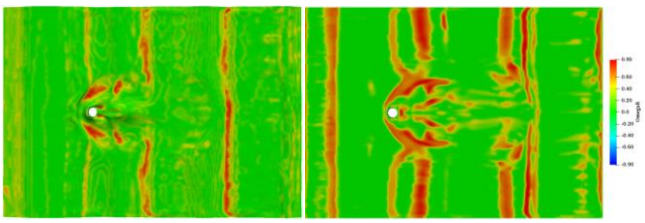

(a) Wave surface (b) 0.5m underwater

Fig. 10 Vorticity distribution of sections at different heights

In order to display the underwater vortex structure, the contour surface of OmegaR = 0.52 is extracted to obtain the underwater vortex distribution by Liutex method, as shown in Fig. 11. The underwater vortex structure is symmetrically distributed. In addition, there are large eddy structures under the water surface, which may be caused by the interaction between surface wave and uniform underwater flow.

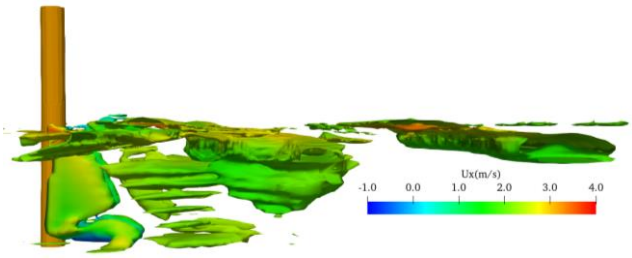

Fig. 11 Instantaneous vorticity distribution behind the cylinder (OmegaR=0.52)

CONCLUSIONS

In this paper, a CFD-FEM solver based on Euler-Bernoulli beam model was developed, and the stability of the solver is preliminarily tested by grid convergence verification. The structural vibration response characteristics of elastic cylinder and hydrodynamic characteristics of flow field under different wave frequencies are studied. Open source software OpenFOAM is used to simulate the flow field, and the turbulence model is chosen as RANS with SST model. Newmark-beta method is applied to calculate the structural field. The main conclusions of this paper are as follows:

For elastic beam, oscillations in the inline direction are more periodic than those in the crossflow direction. When both wave and uniform flow exist at the same time and the wave amplitude is small, different wave frequencies have little effect on the inline direction vibration amplitude after the column vibration is stabilized. And the vibration displacement along crossflow direction is much smaller than that along inline direction.

For fluid field, the existence of uniform flow can highly affect the development of wave, especially when wave amplitude is small. The wave elevation has a run-up ahead of cylinder and a depression behind it. Both wave profile and the underwater vortex structure is symmetrically distributed. Besides, there are large eddy structures under the water surface, which may be caused by the interaction between surface wave and uniform underwater flow.

In particular, this paper only carries out preliminary verification of the FSI solver, and it is necessary to select more typical cases to carry out further verifications.

ACKNOWLEDGEMENTS

This work is supported by the National Natural Science Foundation of China (51809169). This work is also thankful to the cooperation of Marine Design and Research Institute of China.

REFERENCE

Chen, Q., Qi, M. Li, J. (2016). "Kinematic characteristics of horseshoe vortex upstream of circular cylinders in open channel flow." *Journal of Hydraulic Engineering*, 47(2), 158-164.

Ciesielski R, Flaga A, Kawecki J. (1996). "Aerodynamic effects on a non-typical steel chimney 120 m high." *Journal of wind engineering and industrial aerodynamics*. 65, 77-86.

Dargahi, B. (1989). "The turbulent flow field around a circular cylinder." *Experiments in Fluids*, 8, 1-12.

Dean R G, Dalrymple R A. (1991). *Water wave mechanics for engineers and scientists*. World Scientific Press, 16-39.

Ebrahim A, Mohsen S, Ehsan D, Masoud A. (2018). *Archives of Computational Methods in Engineering*, Springer Press, 4-19.

Euler, T., Herget, J. (2012). "Controls on local scour and deposition induced by obstacles in fluvial environments." *CATENA*, 91, 35-46.

Facchinetti, M L, Langre E, Biolley F. (2004). "Coupling of structure and wake oscillators in vortex-induced vibrations." *Journal of Fluids and Structures*, 19(2), 123-140.

Francesca L, Rudiger H, Hans J N. (2021). "Aerodynamic damping in vortex resonance from aeroelastic wind tunnel tests on a stack." *Journal of Wind Engineering and Industrial Aerodynamics*, 208, 104438.

Larsen A. (1995). "A generalized model for assessment of vortex-induced vibrations of flexible structures." *Journal of Wind Engineering and Industrial Aerodynamics*, 57(2), 281-294.

Liang S, Zhou Y, Wang L. (2019). "Wind-induced responses of a high chimney by the wind tunnel tests with a continuous aero-elastic model." *Journal of Vibration and Shock*, 38(10), 149-155.

Liu, J., Liu, C. (2019). "Modified normalized Rortex/vortex identification method." *Physics of Fluids*. 31(6), 61704.

Nikolaos, A, Panayiotis D, Clinton L, Polydefkis B. (2015). "A Time-resolved flow dynamics and Reynolds number effects at a wall–cylinder junction." *Journal of Fluid Mechanics*, 776, 475-511.

Qi, M. (2005). "Riverbed scouring around bridge piers in river section with sand pits." *Journal of Hydraulic Engineering*, 36(7), 835-839.

Tafarojnoruz, A., Gaudio, R., Dey, S. (2010). "Flow-altering countermeasures against scour at ridge piers: a review." *Journal of Hydraulic Research*, 48, 441-452.

Waldeck J. (1992). "The measured and predicted response of a 300 m concrete chimney." *Journal of Wind Engineering and Industrial Aerodynamics*, 41, 229-240.

Yang, P., Zhang, H., Wang, Y. (2019). "Characteristics of horseshoe vortex upstream of a cylinder in shallow water with low cylinder Reynolds number." *Advanced Engineering Sciences*. 51(1), 52–59.

Zhang, R., Xie J. (1989). *Fluvial sediment dynamics*, China Water and Power Press, 5-24.

Zhang Y, Habashi W G, Khurram R A. (2015). "Predicting wind-induced vibrations of high-rise buildings using unsteady CFD and modal analysis." *Journal of Wind Engineering and Industrial Aerodynamics*, 136, 165-179.